Available online at www.sciencedirect.com
SCIENCE DIRECT®
ELSEVIER
Nuclear Instruments and Methods in Physics Research A 519 (2004) 162–174
NUCLEAR INSTRUMENTS & METHODS IN PHYSICS RESEARCH Section A
www.elsevier.com/locate/nima

High-order map treatment of superimposed cavities, absorbers, and magnetic multipole and solenoid fields

K. Makino[a,*], M. Berz[b], C.J. Johnstone[c], D. Errede[a]

[a] *Department of Physics, University of Illinois at Urbana-Champaign, 1110 W. Green Street, Urbana, IL 61801-3080, USA*
[b] *Department of Physics and Astronomy, Michigan State University, East Lansing, MI 48824, USA*
[c] *Fermi National Accelerator Laboratory, P.O. Box 500, Batavia, IL 60510, USA*

Abstract

Various modern systems for the transport and manipulation of large acceptance beams of rare and short-lived particles require the treatment of nonlinear optics of acceleration, absorption, and focusing in a combined approach. We describe a differential algebraic method for the treatment of such nonlinear dynamics via high-order transfer maps. We include the processes of scattering and straggling through absorbing material, which are inherently non-deterministic and hence not representable in the map formalism, in a split operator approach. Some examples of simulations of muon beam ionization cooling channels are provided.

PACS: 02.50.Ey; 02.60.Cb; 02.60.Gf; 02.60.Lj; 05.45.−a; 11.80.La; 29.27.−a; 29.27.Eg; 41.75.Lx; 41.85.−p; 41.85.Ja; 41.85.Lc

Keywords: Transfer map; Nonlinear effect; Differential algebra; Partial differential equation; COSY INFINITY; Muon ionization cooling

1. Introduction

Particle optical systems are usually comprised of electric and magnetic bending elements, focusing elements, and high-order multipoles for correction of aberrations. However, various modern systems for the transport and manipulation of large acceptance beams of rare and short-lived particles require the detailed treatment of more advanced optical elements. In particular, in recent years the reduction of the emittance of such beams has become of prime importance. The systems performing such reduction of emittance usually consist of combinations of absorbers that uniformly reduce the components of the momenta of the particles, as well as cavities that increase predominately the longitudinal components, which overall leads to a reduction of transversal emittance. For purposes of optimal focusing, frequently both cavities and absorbers are placed inside the body or at least the fringe fields of quadrupole or solenoidal focusing elements, which leads to the requirement of treating the nonlinear optics of acceleration, absorption, and focusing in a combined approach.

The treatment of such systems in ray-tracing scenarios based on integration through fields and

*Corresponding author.
E-mail addresses: makino@uiuc.edu (K. Makino), berz@msu.edu (M. Berz), cjj@fnal.gov (C.J. Johnstone), derrede@uiuc.edu (D. Errede).

0168-9002/$ - see front matter © 2003 Elsevier B.V. All rights reserved.
doi:10.1016/j.nima.2003.11.133

matter is very laborious and time consuming, and does not lend itself well to optimization and correction of undesirable nonlinear effects. We describe a differential algebraic (DA) method [1–3] for the treatment of such nonlinear dynamics, based on the spatial and temporal form of the accelerating fields, any superimposed focusing magnetic fields, and the geometry and physical properties of the absorbing material and its possible vessel. Described by a Bethe–Bloch–Vavilov formalism [4], the bulk of the effects is described in terms of a high-order nonlinear transfer map. The also occurring scattering and straggling [4–6], which are inherently non-deterministic and hence not representable in the map formalism, are described in terms of a set of stochastic kicks in the transversal and longitudinal dynamics. The stochastics is propagated to the center of the occurring absorbers and thus allows a combined treatment of the tracking of both deterministic and random effects in an efficient way. The method is implemented in the high-order code COSY INFINITY [7]. Examples for the application and performance of the method are given, using muon beam ionization cooling channels [8,9].

We start the discussion with the DA methods and the DA PDE (partial differential equation) solvers, which provide an efficient mechanism to treat complicated nonlinear electromagnetic fields.

2. DA PDE solvers

The differential algebraic DA methods [1–3] allow the efficient computation and manipulation of high-order Taylor transfer maps. When integrating transfer maps through electromagnetic fields, the full 3D fields are computed as part of each integration time step using DA PDE solvers. In this section, we address the mechanism of the method of DA PDE solvers.

First, we introduce the basics of the DA methods briefly to the extent necessary for discussing the DA fixed point PDE solvers. The idea of DA methods is based on the observation that it is possible to extract more information about a function than its mere values on computers. One can introduce an operation T as the extraction of the Taylor coefficients of a prespecified order n of the function. In mathematical terms, T is an equivalence relation, and the application of T corresponds to the transition from the function to the equivalence class comprising all those functions with identical Taylor expansion to order n. Since Taylor coefficients of order n for sums and products of functions as well as scalar products with reals can be computed from those of the summands and factors, the set of equivalence classes of functions can be endowed with well-defined operations, leading to the so-called Truncated Power Series Algebra (TPSA) [10,11]. The development of algorithms for functions followed, including methods to perform composition of functions, to invert them, and to introduce the treatment of common elementary functions. The power of TPSA can be enhanced by the introduction of derivations ∂ and their inverses ∂^{-1}, corresponding to the differentiation and integration on the space of functions, resulting in a differential algebra [1,2,12,13], which allows the direct treatment of many questions connected with differentiation and integration of functions, including the solution of the ODEs $d\vec{x}/dt = \vec{f}(\vec{x}, t)$ [14] describing the motion and PDEs describing the fields.

2.1. The differential algebra ${}_nD_v$ and the DA fixed point theorem

For the purpose of further discussion, we briefly review a differential algebra that allows to compute derivatives up to order n of functions in v variables. On the space $C^n(R^v)$, we introduce an equivalence relation. For f and g in $C^n(R^v)$ we say $f =_n g$ if and only if $f(0) = g(0)$, and all the partial derivatives of f and g agree at 0 up to order n. The relation $=_n$ is an equivalence relation. We group all those elements that are related to f together in one set, the equivalence class $[f]$ of the function f. The resulting equivalence classes are often also referred to as DA vectors or DA numbers. Intuitively, each of these classes is then specified by a particular collection of partial derivatives in all v variables up to order n. We call the collection of all these classes ${}_nD_v$. For more details, see Ref. [1].

To any element $[f]\in {}_nD_v$ we define the depth $\lambda([f])$ as

$$\lambda([f]) = \begin{cases} \text{Order of first non-vanishing} \\ \text{derivative of } f & \text{if } [f]\neq 0 \\ n+1 & \text{if } [f]=0. \end{cases}$$

In particular, any function f that does not vanish at the origin has $\lambda([f])=0$. In a similar way, on the set $({}_nD_v)^m$ that describes vector functions $\vec{f} = (f_1,\ldots,f_m)$ from R^v to R^m, we define

$$\lambda(([f_1],\ldots,[f_m])) = \min_{1\leqslant k\leqslant m} \lambda([f_k]).$$

Let $\mathcal{O}$ be an operator on the set $M\subset({}_nD_v)^m$. Then we say that $\mathcal{O}$ is contracting on M if for any $\vec{a}$, $\vec{b}\in M$ with $\vec{a}\neq\vec{b}$,

$$\lambda(\mathcal{O}(\vec{a})-\mathcal{O}(\vec{b})) > \lambda(\vec{a}-\vec{b}).$$

In practical terms this means that after application of $\mathcal{O}$, the derivatives in $\vec{a}$ and $\vec{b}$ agree to a higher order than before application of $\mathcal{O}$. For example, the antiderivation ∂_k^{-1} is a contracting operator.

Contracting operators have a very important property, namely they satisfy a fixed point theorem.

Theorem 1 (DA fixed point theorem). *Let $\mathcal{O}$ be a contracting operator on $M\subset {}_nD_v$ that maps M into M. Then $\mathcal{O}$ has a unique fixed point $a\in M$ that satisfies the fixed point problem*

$$a=\mathcal{O}(a).$$

Moreover, let a_0 be any element in M. Then the sequence

$$a_k=\mathcal{O}(a_{k-1}) \quad \text{for } k=1,2,\ldots$$

converges in finitely many steps (in fact, at most $(n+1)$ steps) to the fixed point a.

The fixed point theorem is of great practical usefulness since it assures the existence of a solution, and moreover allows its exact determination in a very simple way in finitely many steps. The proof of the theorem can be found in Ref. [1].

The fixed point theorem and its proof have many similarities to its famous counterpart due to Banach on Cauchy-complete normed spaces. In the DA version of the fixed point theorem, convergence happens even very conveniently already after finitely many steps. Similar to the case of the Banach fixed point theorem, also the DA fixed point theorem has many useful applications, in particular a rather straightforward solution of ODEs and PDEs.

2.2. DA fixed point PDE solvers

The direct availability of the derivation ∂ and its inverse ∂^{-1} allows to devise efficient numerical PDE solvers of any order. The DA fixed point theorem allows to solve PDEs iteratively in finitely many steps by rephrasing them in terms of a fixed point problem. The details depend on the PDE at hand, but the key idea is to eliminate differentiation with respect to one variable and replace it by integration. As an example, consider the rather general PDE

$$a_1\frac{\partial}{\partial x}\left(a_2\frac{\partial}{\partial x}V\right)+b_1\frac{\partial}{\partial y}\left(b_2\frac{\partial}{\partial y}V\right) + c_1\frac{\partial}{\partial z}\left(c_2\frac{\partial}{\partial z}V\right)=0$$

where a_1, a_2, b_1, b_2, c_1, c_2 are functions of x, y, z. The PDE is re-written as

$$V = V|_{y=0} + \int_0^y \frac{1}{b_2}\left(b_2\frac{\partial V}{\partial y}\right)\Big|_{y=0} \mathrm{d}y - \int_0^y \frac{1}{b_2}\int_0^y \left(\frac{a_1}{b_1}\frac{\partial}{\partial x}\left(a_2\frac{\partial V}{\partial x}\right) + \frac{c_1}{b_1}\frac{\partial}{\partial z}\left(c_2\frac{\partial V}{\partial z}\right)\right)\mathrm{d}y\,\mathrm{d}y.$$

The equation is now in fixed point form. The partial derivative operators $\partial/\partial x$ and $\partial/\partial z$ act to evaluate the regular partial derivatives in DA. Now assume the derivatives of V and $\partial V/\partial y$ with respect to x and z are known in the plane $y=0$. If the right-hand side is contracting with respect to y, the various orders in y can be iteratively calculated by mere iteration. We will now consider various versions of the operators and try to assess contractivity.

As a particularly important example, consider the Laplace equation. It can be represented in general curvilinear coordinates [15,16]. In the

special case of a planar curvilinear coordinate system, the Laplace equation is obtained as [15,16]

$$\Delta V = \frac{1}{1+hx}\frac{\partial}{\partial x}\left\{(1+hx)\frac{\partial V}{\partial x}\right\} + \frac{\partial^2 V}{\partial y^2} + \frac{1}{1+hx}\frac{\partial}{\partial s}\left(\frac{1}{1+hx}\frac{\partial V}{\partial s}\right) = 0.$$

In the case of a straight section, where $h = 0$, it reduces to nothing but the Cartesian Laplace equation. The fixed point form of the Laplace equation in the planar curvilinear coordinates is

$$V = V|_{y=0} + \int_0^y \left(\frac{\partial V}{\partial y}\right)\Big|_{y=0} \mathrm{d}y - \int_0^y \int_0^y \left[\frac{1}{1+hx}\frac{\partial}{\partial x}\left\{(1+hx)\frac{\partial V}{\partial x}\right\} + \frac{1}{1+hx}\frac{\partial}{\partial s}\left(\frac{1}{1+hx}\frac{\partial V}{\partial s}\right)\right] \mathrm{d}y\mathrm{d}y. \quad (1)$$

In this form, the right-hand side has the interesting property that, regardless of what function V is inserted, the parts not depending on y are reproduced exactly, since all integrals introduce y dependence. Thus considering the subspace comprising $V(y)$ for a given choice of x and s, the right hand side is contracting. In COSY INFINITY [7], the planar curvilinear Laplace equation is solved by the following very compact code:

```
POLD := P;
HF := 1+H*DA(IX);
HI := 1/HF;
LOOP I 2 NOC+2 2;
 P := POLD - INTEG(IY,INTEG(IY,
    HI*(DER(IX,HF*DER(IX,P))
 + DER(IS,HI*DER(IS,P)))));
 ENDLOOP;
```

where the boundary condition $V|_{y=0} + \int_0^y (\partial V/\partial y)\big|_{y=0} \mathrm{d}y$ is provided through the incoming `P` using the DA expression in COSY. The DA fixed point iteration converges to the solution potential `P` in finitely many steps. `DA(IX)` represents the identity for x, `NOC` is the current transfer map computation order, and `DER(I,...)` and `INTEG(I,...)` correspond to the DA derivative and the DA anti-derivative operations with respect to the variable specified by the first argument `I`, namely "∂_{x_I}" and "$\int_0^{x_I} \mathrm{d}x_I$". The full 3D field is derived from the solution potential `P`, using again the DA technique as

```
BX := DER(IX,P);
BY := DER(IY,P);
BZ := DER(IS,P);
```

The advantages of the method are:

- One needs code for the field only for the midplane.
- The resulting field will always satisfy stationary Maxwell's equations.
- It works to any order.

As a simple but illuminating example that can be done by hand, let us consider the s-independent potential of an electric quadrupole in Cartesian coordinates. From Eq. (1), the fixed point form of the Laplace equation is

$$V = V|_{y=0} + \int_0^y \left(\frac{\partial V}{\partial y}\right)\Big|_{y=0} \mathrm{d}y - \int_0^y \int_0^y \frac{\partial^2 V}{\partial x^2} \mathrm{d}y\,\mathrm{d}y.$$

We have $V|_{y=0} = Mx^2$ and $(\partial V/\partial y)\big|_{y=0} = 0$ as the boundary condition. Since $\partial^2 V/\partial x^2 = 2M$, $\int_0^y \int_0^y \partial^2 V/\partial x^2 \,\mathrm{d}y\,\mathrm{d}y = My^2$, thus the evaluation of the right-hand side provides $M(x^2 - y^2)$, which is the expression of the potential after one iteration $V_{(1)}$. The application of the fixed point operator to $V_{(1)}$ gives the same result as $V_{(1)}$, thus the DA fixed point iteration converged, and the solution potential is $V = M(x^2 - y^2)$.

Another important coordinate system often suitable for computations under consideration are the cylindrical coordinates, for which the Laplace equation is

$$\Delta V = \frac{1}{r}\frac{\partial}{\partial r}\left(r\frac{\partial V}{\partial r}\right) + \frac{1}{r^2}\frac{\partial^2 V}{\partial \phi^2} + \frac{\partial^2 V}{\partial s^2} = 0.$$

If V does not depend on ϕ, namely V is rotationally symmetric, as in solenoid magnets, the fixed point form of the Laplace equation is simplified to

$$V = V|_{r=0} - \int_0^r \frac{1}{r}\int_0^r r\frac{\partial^2 V}{\partial s^2} \mathrm{d}r\,\mathrm{d}r$$

and the right-hand side is contracting with respect to r. Since we are only interested in cases in which

$V(r,s)$ is expressed in DA, if $\partial^2 V/\partial s^2$ is non-zero, the integral $\int_0^r r\partial^2 V/\partial s^2\,\mathrm{d}r$ contains r to a positive power. Thus, the factor $1/r$ in the outer integral simply lowers the power of r by one, and the right-hand side of the fixed point form can be evaluated in DA without posing trouble. To perform the DA fixed point iteration for the purpose of obtaining the full potential $V(r,s)$, one only needs to prepare the on-axis potential expression $V(r,s)|_{r=0}$ as the boundary condition.

2.3. Example

For solenoid magnets, the DA PDE solver only requires the analytical expression of the potential on axis, as seen in the last section. For various practical systems, it can even be usually easily described. For example, the on-axis longitudinal field and the on-axis potential of a thin solenoid, namely a solenoid with zero thickness, are explicitly given as [17]

$$B_z(s) = \frac{\mu_0 In}{2}\left(\frac{s}{\sqrt{s^2+R^2}} - \frac{s-L}{\sqrt{(s-L)^2+R^2}}\right)$$

$$V(s) = \frac{\mu_0 In}{2}\left(\sqrt{s^2+R^2} - \sqrt{(s-L)^2+R^2}\right)$$

where R is the radius, I is the current in the coil, n is the number of turns per unit s-direction length, and the coil extends from $s=0$ to L. If the solenoid is infinitely long, i.e. $L \gg R$, the field in the middle of the solenoid approaches the asymptotic value $B_z(L/2) \to \mu_0 In$. While this on-axis form is easily obtained, the out of axis form cannot be represented in closed form as it involves elliptic integrals [18]; thus the ability of the DA PDE solver to generate the power series representation of the field to any order is very useful.

Using a part of the code ICOOL [19,20] for the field computation of a thin solenoid with elliptic integrals [18], we computed the 3D fields of a thin solenoid with $L = 1$ m and $R = 0.3$ m and the current density In adjusted to $\mu_0 In = 1$ T, and the result was compared with that of the DA PDE solver using the code COSY INFINITY. In the range of longitudinal position s from -1 m to $L + 1$ m $= 2$ m, the on-axis longitudinal field has agreement to nearly machine precision between ICOOL and COSY INFINITY; the field profile is shown in the left picture in Fig. 1. The longitudinal and the transversal fields B_z and B_r are evaluated in ICOOL and COSY INFINITY over the longitudinal position from -1 to 2 m at every 0.05 m position at various radii, and the average differences are plotted as a function of the expansion order of the fields computed by the DA PDE solver at 60%, 70%, 80% and 90% of the full radius R in the right

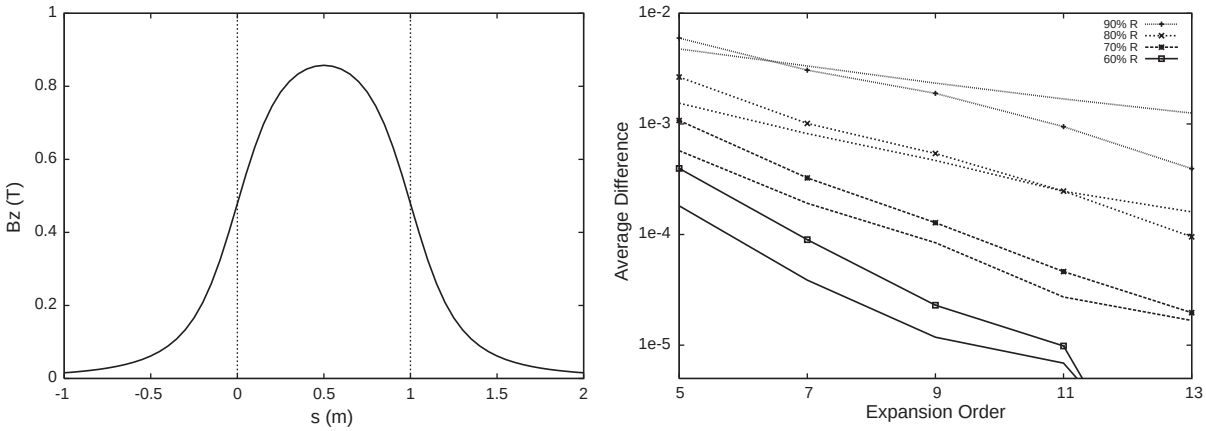

Fig. 1. The axial field profile of a thin solenoid with $L = 1$ m and $R = 0.3$ m (left). The DA PDE solver is compared with the computation with elliptic integrals (right). At various radii (90%, 80%, 70% and 60% of R downward), the differences in B_z (with marks) and B_r (without marks) over the range from $s = -1$ to 2 m are averaged.

picture in Fig. 1. In the picture, the average differences of B_z is shown with marks, and B_r is shown without marks.

The decrease of the differences as the expansion order increases shows the expected decrease of error with order. The fact that the curves are nearly linear shows that the dependence is nearly of the form a^n, where the logarithm of a corresponds to the slope of the curves. It is apparent that the larger the ratio of radius to aperture of the coil becomes, the smaller the slope becomes. Extrapolation of the visible slopes suggests that zero slope is achieved close to the case where radius equals aperture, and thus the radius of convergence of the power series is nearly the aperture.

More quantitatively, at 90% of the full radius R, the average differences are much less than 1%, and the average differences of B_r tend to be larger than those of B_z, differing from the smaller radius cases. This is attributed to diverging values of B_r computed by ICOOL when the radius gets close to the full radius R at the end positions of the solenoid ($s = 0$ and 1 m).

Since the solenoid field computation using elliptic integrals in ICOOL is limited to thin solenoids, it is necessary to overlay several of them to represent a thick solenoid in ICOOL. Because of the inherently approximate nature of the results, we did not perform a one-to-one comparison of field computations for a thick solenoid.

While analytical expression of on-axis field and potential of solenoids can be obtained theoretically, this is not the case for multipoles where the actual current wiring affects the longitudinal end field profile. However, once appropriate boundary conditions to the DA PDE solver are provided, namely an on-axis potential for a magnetic multipole, and B_y in the midplane for a magnetic dipole, the similar level of performance comparable to the above solenoid example is expected by the off-axis or the off-plane expansion. The Enge function is widely used to describe such longitudinal end field profile, and the function is easy to handle, but any expression which fits into the framework of DA can be used to describe such boundary conditions to the DA PDE solver.

3. Superimposed solenoids

In practice, solenoids have non-zero thickness, and often even very thick solenoids are used as in the case of an sFOFO muon beam ionization cooling cell as described in Table 1 and Fig. 3. As a preparation for the treatment of general solenoidal fields, we describe a single solenoid with non-zero thickness, the on-axis longitudinal field of which is given by the following expression [17]:

$$B_z(s) = \frac{\mu_0 In}{2(R_2 - R_1)} \left\{ s \log\left(\frac{R_2 + \sqrt{R_2^2 + s^2}}{R_1 + \sqrt{R_1^2 + s^2}} \right) - (s - L) \log\left(\frac{R_2 + \sqrt{R_2^2 + (s-L)^2}}{R_1 + \sqrt{R_1^2 + (s-L)^2}} \right) \right\}$$

where R_1 and R_2 are the inner and outer radii. If the solenoid is infinitely long, i.e. $L \gg R_1, R_2, (R_2 - R_1)$, the field approaches the asymptotic value $B_z(L/2) \to \mu_0 In$. The on-axis potential expression can be derived easily from the above field expression by integration with respect to s as

$$V(s) = \frac{\mu_0 In}{4(R_2 - R_1)} \left\{ s^2 \log\left(\frac{R_2 + \sqrt{R_2^2 + s^2}}{R_1 + \sqrt{R_1^2 + s^2}} \right) - (s - L)^2 \log\left(\frac{R_2 + \sqrt{R_2^2 + (s-L)^2}}{R_1 + \sqrt{R_1^2 + (s-L)^2}} \right) + R_2 \sqrt{R_2^2 + s^2} - R_1 \sqrt{R_1^2 + s^2} - R_2 \sqrt{R_2^2 + (s-L)^2} + R_1 \sqrt{R_1^2 + (s-L)^2} \right\}.$$

Table 1
Properties of the coils in a 2.75 m sFOFO cell [8]

Position s (m)	Length L (m)	Inner radius R_1 (m)	Thickness $R_2 - R_1$ (m)	Current density j (A/mm^2)
0.175	0.167	0.330	0.175	75.20
1.210	0.330	0.770	0.080	98.25
2.408	0.167	0.330	0.175	75.20

Compared to the asymptotic field strength $\mu_0 In$, the field strength is much lower for solenoids, in which $L \approx R$. It is interesting that in case of thick solenoids, the characteristic aperture is the outer radius R_2, rather than the inner radius R_1 [17]. The left picture in Fig. 2 shows the relative field strength compared to the ideal strength $\mu_0 In$ for a thin solenoid with the equal length and diameter, i.e. $L = 2 \cdot R$. The actual size, which is irrelevant here, is chosen to $L = 0.6$ m, representing the size of magnets used in the quadrupole muon beam ionization cooling cell as shown in Fig. 5. In this case the relative field strength reaches only to 71% ($= 1/\sqrt{2}$), and the fringe field extends for a long distance; for example, at the outside point L away from the solenoid, the relative field strength still maintains 4%.

The major idea in some of the current designs of various muon beam ionization cooling channels is to use strong solenoids to guide the beams with large transversal emittance. Those solenoids are planned to have very large aperture such that cavities and absorbers can be nested inside, which makes the fringe field extension longer and the maximum field strength lower, and altogether the thickness of the coils becomes quite large. As a result, the fringe field extends yet farther, and the entire solenoid is comprised of "fringe" fields. An approximation based on $B_z(s) \propto [\tanh(s/R) - \tanh((s-L)/R)]$ is commonly adopted for describing an on-axis solenoid field, because it drops more swiftly in the fringe region compared to the pure theoretical field, making the simulation effort easier. On the other hand, the discrepancy from the actual field becomes very large particularly for thick solenoids [17], which are important in practice to provide high field strength.

As an example of superposition of several thick solenoids, we present a 2.75 m sFOFO muon beam ionization cooling cell in Muon Feasibility Study II [8]. Table 1 lists the geometry and current densities of the coils in the cell, and the pictures in Fig. 3 show the coil layout and the axial field profile as well as the field distributions $B_z(r,s)$, $B_r(r,s)$ that are obtained via the DA fixed point PDE solver. There are three coils in the cell, and the thickness is very large. As a result, the superimposed field maintains high strength throughout the cell except for the ends of the cell, where the axial field drops to zero due to the alternating field direction in the preceding and following cells.

4. Cells consisting of magnets, cavities and absorbers

The sFOFO muon beam ionization cooling cell discussed above includes accelerating cavities and absorbers as illustrated in Fig. 4 [8]. The absorbers reduce the transversal and longitudinal components of momenta of muons uniformly, and the

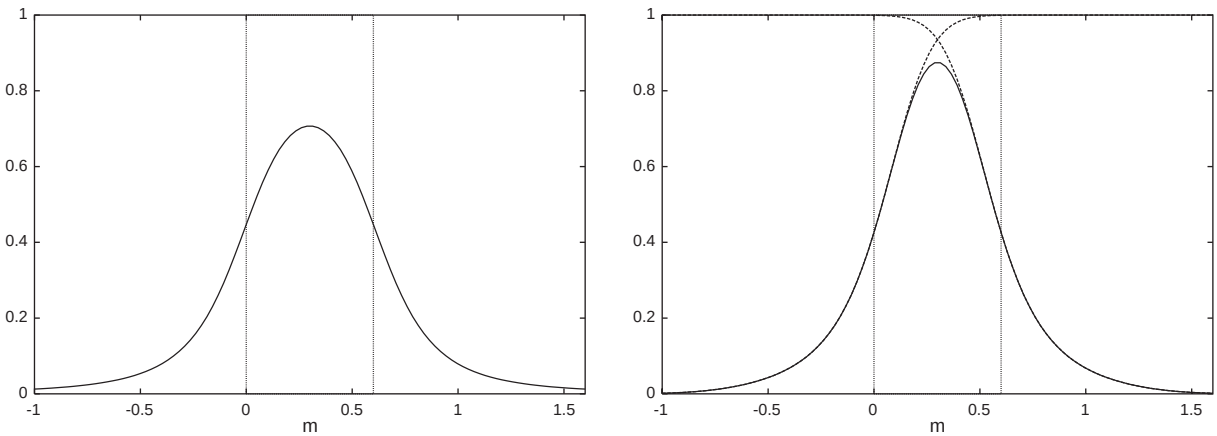

Fig. 2. The fringe field extension of a solenoid (left) and an example quadrupole (right) of the same geometry. The length is equal to the diameter, and both are 60 cm. The field strength is relative to the infinitely long case.

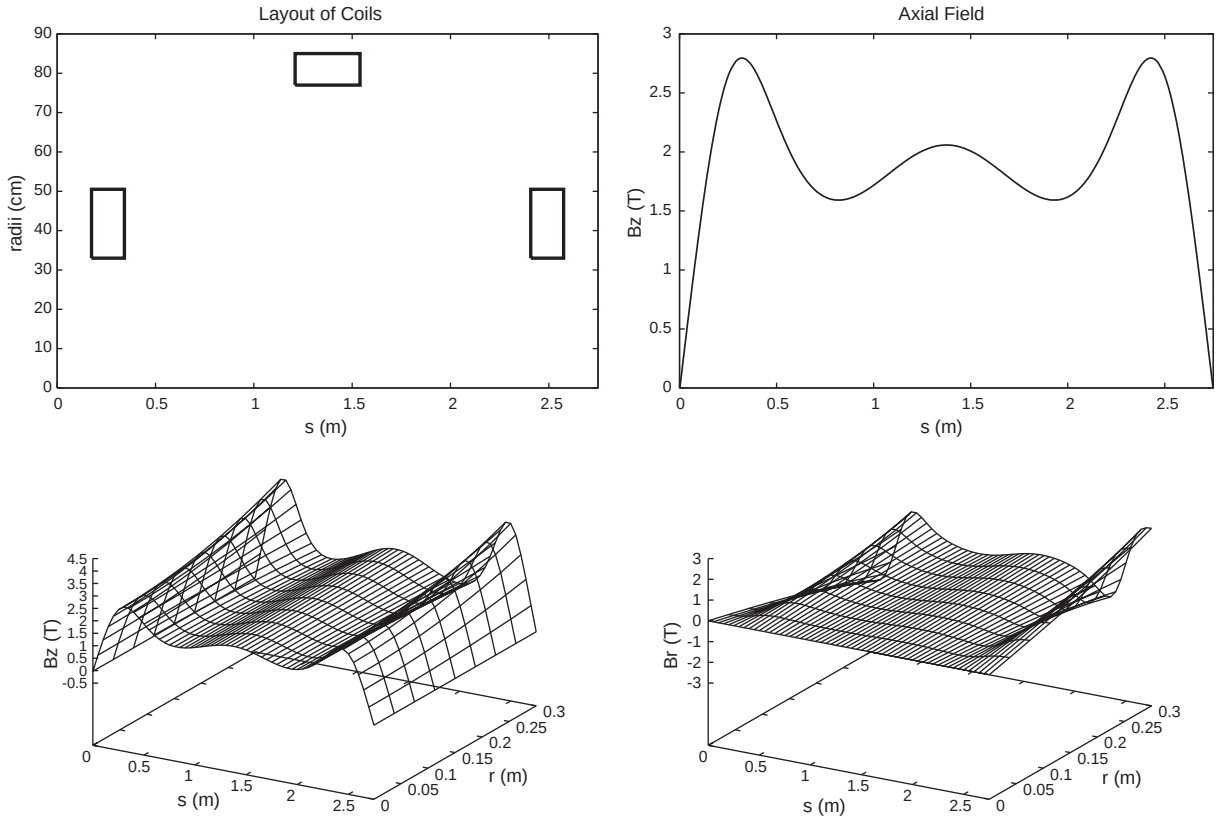

Fig. 3. The coil layout, the axial field profile $B_z(s)$, and the field distribution $B_z(r,s)$, $B_r(r,s)$ of a 2.75 m sFOFO cell. The full 3D field distributions $B_z(r,s)$, $B_r(r,s)$ are derived only from the on-axis potential $V(s) = \int_s B_z(s)$ using the DA fixed point PDE solver.

accelerating cavities increase the longitudinal components, thus achieving the desired ionization cooling in the cell. Both the absorbers and the cavities are situated in the superimposed solenoidal field, and the axial field strength drops to zero in the middle of the absorbers. The need to combine the cavities, the absorbers and the guiding magnetic fields together requires the solenoids to have very large aperture and high current. This kind of nested layout of different elements is typical of muon ionization cooling cell designs using solenoids as focusing magnets. While the idea is against the modern concept for designing beam optical systems with single function elements, we can treat such systems with transfer maps in the frequently used split operator approach, which is based on the fact that for operators A, B we have $\exp(A+B) \approx \exp(A) \cdot \exp(B)$. The approximation holds to second order in the norms of A and B and is a simple consequence of the Baker Campbell Hausdorff formula for exponentials of non-commuting operators.

For the specific case at hand, the operator describes the flow of the ODE, the solution of which is written as an exponential of the directional derivative operator. The operator consists of three parts, one describing the action of the field-free drift D, including all higher order terms sometimes referred to as the kinematic correction, the field contributions due to the solenoid S, and the field contributions due to the cavity C. The solution for the time step Δt is now first split into N parts as

$$\exp(\Delta t \cdot (D+S+C)) = \prod_{i=1}^{N} \exp\left(\frac{\Delta t}{N} \cdot (D+S+C)\right)$$

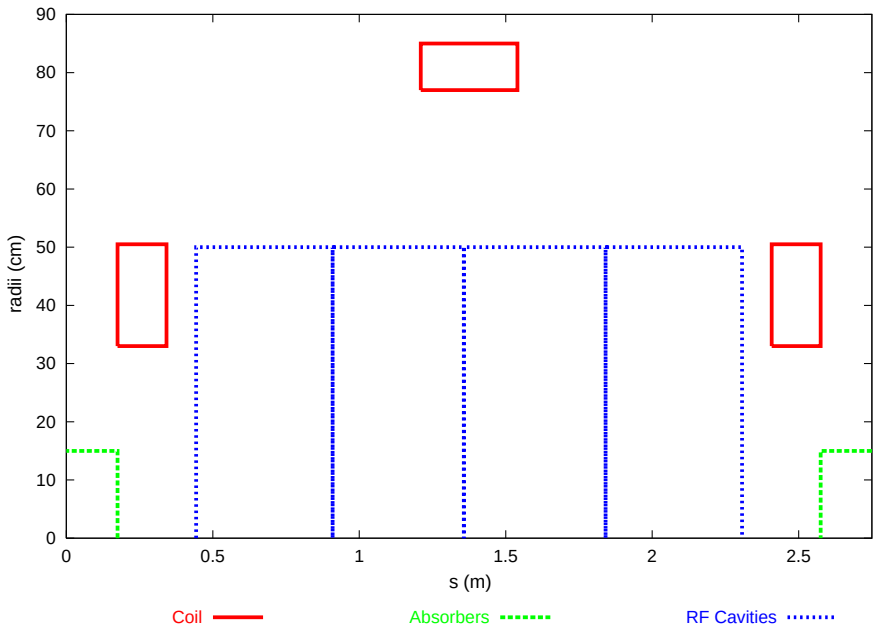

Fig. 4. The layout of the 2.75 m sFOFO muon beam ionization cooling cell.

and then for each of these parts, the split-operator technique is applied as

$$\exp\left(\frac{\Delta t}{N}\cdot(D+S+C)\right)$$
$$=\exp\left(\frac{\Delta t}{N}\cdot((D+S)+(-D)+(D+C))\right)$$
$$\approx\exp\left(\frac{\Delta t}{N}\cdot(D+S)\right)\cdot\exp\left(\frac{\Delta t}{N}\cdot(-D)\right)$$
$$\cdot\exp\left(\frac{\Delta t}{N}\cdot(D+C)\right).$$

The end result consists of short flows of the ODEs for a negative plain drift $\exp(\Delta t/N(-D))$, a plain solenoid $\exp(\Delta t/N(D+S))$, as well as a plain cavity $\exp(\Delta t/N(D+C))$, all of which are directly available within the framework of the code COSY INFINITY.

So in practice, the cell under consideration is sliced into short pieces that are solved separately, and the superposition of the separate pieces is achieved by inserting suitable negative drifts. For example, the 2.75 m sFOFO cell is sliced into about 80 pieces. We note that when in advanced stages of design, more information of the details of the cavity fields are known, and a higher degree of accuracy is required, it is also possible to directly integrate through the superposition of these fields, in a way similar to Refs. [21,22].

If we can avoid the nesting of different beam optical elements, the treatment of the systems can be simplified. The following robust quadrupole muon beam ionization cooling cell is such an example; the cell consists of alternating short magnetic quadrupoles, cavities and absorbers without nesting [9] (Fig. 5). In this design, each element can be treated independently as a single function element. Because of the large transversal emittance of muon beams, the aperture is set to be 30 cm radius, comparable to that of the sFOFO cell. For the purpose of keeping the total size of the cell small, the length of the magnetic quadrupoles is chosen to be 60 cm. The ratio of length to aperture of the quadrupoles is comparable to that of the solenoid discussed earlier for Fig. 2, i.e. the length is equal to the diameter, and the whole field is dominated by the fringe fields. At this early design stage, we use a set of standard data for the fringe field fall off, which is based on the measurement of PEP/SLAC magnets [7,23]. The

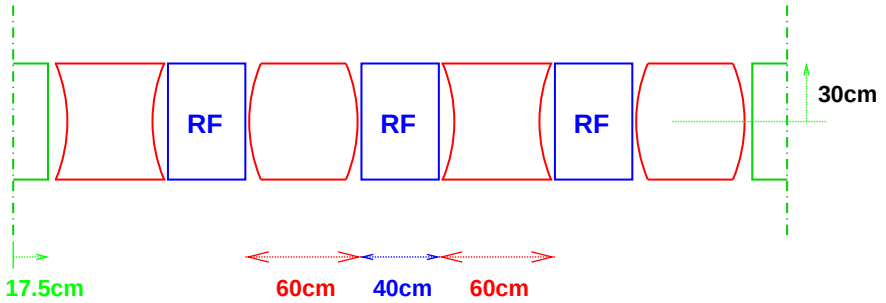

Fig. 5. The layout of a quadrupole muon beam ionization cooling cell [9].

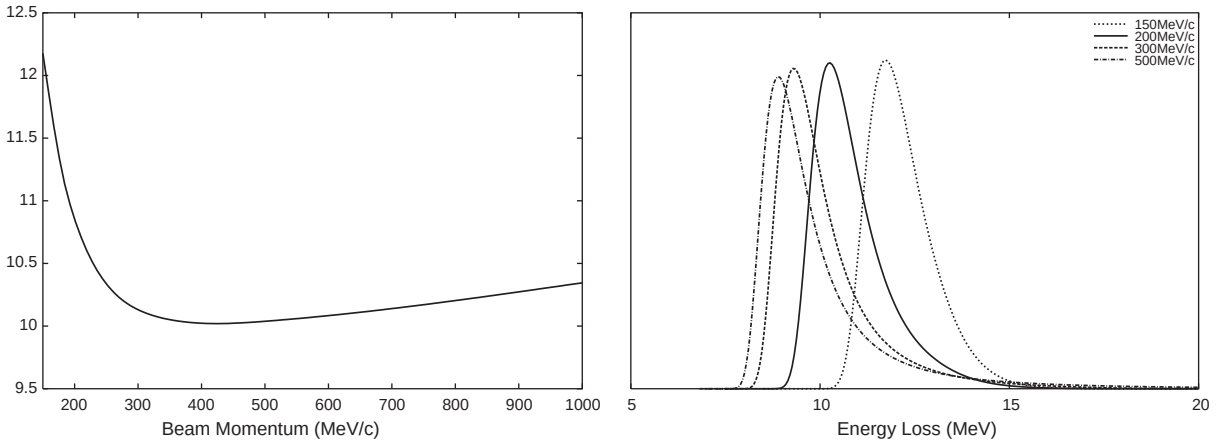

Fig. 6. The mean energy loss (left) and the Vavilov energy loss distribution (right) of muon beams going through 35 cm liquid hydrogen.

points to be stressed here are that the fringe field consideration has to be included from the beginning stage of the cell design as we do, although the effects of the fringe field is much more benign than those for solenoids allowing the single function element treatment in the transfer map approach. It also should be noted that the pole tip field strength is about 0.5 T, thus the magnets can be built without having to resort to superconducting coils.

5. Differential algebraic treatment of dynamics through material

To treat microscopic phenomena happening when charged particle beams go through absorbing material, the average of changes is taken as deterministic macroscopic phenomena to be included in the description of dynamics by transfer maps. By its nature, the transfer map approach assumes deterministic motion, and thus non-deterministic random effects happening when going through material cannot be represented in the standard manner. In this section, we describe how to combine those two conflicting phenomena in transfer map-based simulations.

The deterministic effect of passing through material is the mean energy loss, and it is characterized by the Bethe–Bloch formula

$$-\frac{\mathrm{d}E}{\mathrm{d}x} = 2\pi N_a r_e^2 m_e c^2 \rho \frac{Z}{A}\frac{z^2}{\beta^2}\left[\ln\left(\frac{2m_e\gamma^2 v^2 W_{\max}}{I^2}\right) - 2\beta^2 - \delta - 2\frac{C}{Z}\right]$$

where r_e is classical electron radius, I is mean excitation potential, W_{max} is the maximum energy transfer in a single collision, δ is the density correction, and C is a shell correction [4]. The left picture in Fig. 6 shows the mean energy loss of muon beams going through 35 cm liquid hydrogen as a function of the incoming beam momentum. The 2.75 m sFOFO cell has an absorber section consisting of 35 cm of liquid hydrogen and a vessel with two aluminum windows with a minimum thickness of 300 μm at the center [8,24]. The absorbers of the same material and of the same

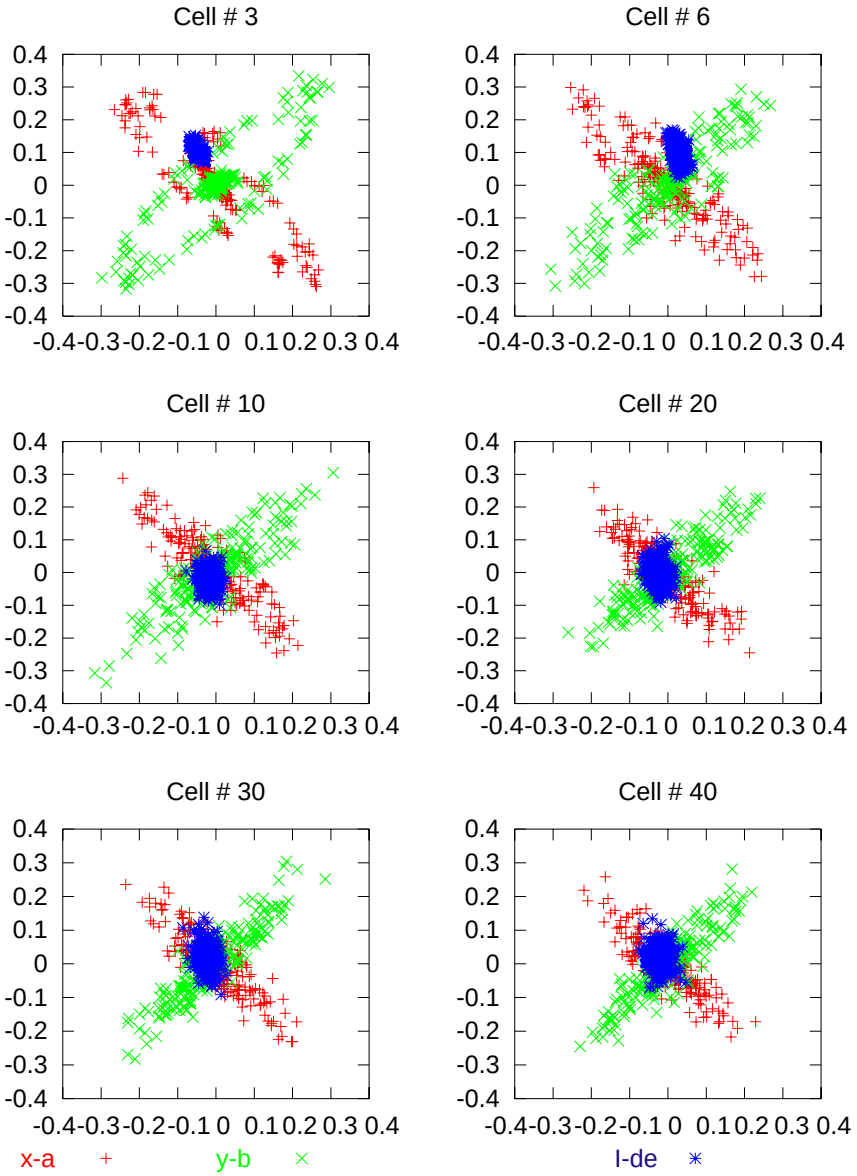

Fig. 7. Muon beam tracking through the quadrupole muon beam ionization cooling cells. Random processes due to multiple scattering and straggling are included in the Monte Carlo approach.

thickness are used for the quadrupole cooling cells, too [9]. Once the geometry and the physical properties of the absorber are determined, the mean energy loss through the absorber is determined uniquely based on the mass, charge, and spin, and the phase space coordinates of the incoming particle, and thus can be included into the transfer map of the system.

The incoming muon beam momentum ranges from 150 to 400 MeV/c, and we consider the following two non-deterministic random processes. One is multiple scattering, a transversal effect, and the other is energy straggling, a longitudinal effect [5,6,24]. We treat the random effects as a set of stochastic kicks in the dynamics. In a similar manner, muon decay can be treated, but because of its relatively low rate, it is not included in our current simulations [9,24] at this time. The multiple scattering is represented by a random kick in the transversal components of momenta, and the kick follows a Gaussian distribution centered at zero. We denote this random event as $\mathscr{R}_{\mathrm{MS}}$. The straggling is a set of random kicks in energy, and the kicks have an energy loss distribution depending on the thickness and physical properties of material and the kind and energy of incoming particles. We denote it as $\mathscr{R}_{\mathrm{St}}$. In the absorbers under consideration, the distribution follows Vavilov's theory [4–6,24], and is shown in the right picture in Fig. 6 in case of 35 cm liquid hydrogen.

The random kicks are treated in a Monte Carlo approach. The transversal kicks have a Gaussian distribution, so a set of Gaussian random numbers are generated for horizontal and vertical components of momentum. The longitudinal kicks have a complicated asymmetric distribution, so random numbers following this distribution are generated for energy loss. We include the stochastic kicks in the dynamics through tracking. For efficiency, we describe all stochastic effects by kicks longitudinally placed in the middle of the absorber. In order to match, the cell starts and ends in the middle of the absorber, and we first prepare the deterministic high-order transfer map $\mathscr{M}$ of the cell, where the cavities are driven to replenish the mean energy lost in the absorber. A set of particles is tracked via the high-order map for the cell; then the Monte Carlo kicks are executed, so that

$$\vec{z}_f = (\mathscr{R}_{\mathrm{MS}} \circ \mathscr{R}_{\mathrm{St}} \circ \mathscr{M})(\vec{z}_i).$$

Again this approach is based on the split operator method, except that here, the straggling and multiple scattering terms are localized only within the absorber which comprises only a small fraction of the entire lattice. Thus if any subdivision is needed at all, it is limited to a short part of the system under consideration. This procedure is iterated for the next cell. The tracking pictures in Fig. 7 show an example of the method for the quadrupole muon beam ionization cooling channel. The initial distribution of 200 MeV/c muons is prepared to fill the maximum transversal beam acceptance without longitudinal distribution. The particle distribution is plotted using the symbols "+", "×" and "★" for the horizontal, vertical and longitudinal phase space after various numbers of repetition of the cell, respectively. Transversal beam cooling effect is observed, while the longitudinal emittance reaches an equilibrium quickly.

Acknowledgements

We would like to thank two anonymous referees for various useful comments, and Stephen Kahn for providing the information on the thin solenoid field computation with elliptic integrals used in ICOOL. The work was supported by the Illinois Consortium for Accelerator Research, the US Department of Energy, an Alfred P. Sloan Fellowship and the National Science Foundation.

References

[1] M. Berz, Modern Map Methods in Particle Beam Physics, Academic Press, San Diego, 1999.
[2] M. Berz, Part. Accel. 24 (1989) 109.
[3] M. Berz, K. Makino, New approaches for the validation of transfer maps using remainder-enhanced differential algebra, Nucl. Instr. and Meth., 2004, these proceedings.
[4] W.R. Leo, Techniques for Nuclear and Particle Physics Experiments: A How-to Approach, Springer, Berlin, New York, 1987, 1994.
[5] A. van Ginneken, Nucl. Instr. and Meth. A 362 (1995) 213.
[6] A. van Ginneken, Nucl. Instr. and Meth. B 160 (2000) 460.

[7] M. Berz, K. Makino, COSY INFINITY Version 8.1—user's guide and reference manual, Technical Report MSUHEP-20704, Department of Physics and Astronomy, Michigan State University, East Lansing, MI 48824, 2001, See also http://cosy.pa.msu.edu.
[8] S. Ozaki, R. Palmer, M. Zisman, J. Gallardo (Eds.), Feasibility study—II of a muon-based neutrino source, Technical Report 52623, Muon Collider Collaboration, BNL, 2001.
[9] C.J. Johnstone, M. Berz, D. Errede, K. Makino. Muon beam ionization cooling in a linear quadrupole channel, Nucl. Instr. and Meth., 2004, these proceedings.
[10] M. Berz, The new method of TPSA algebra for the description of beam dynamics to high orders, Technical Report AT-6:ATN-86-16, Los Alamos National Laboratory, 1986.
[11] M. Berz, Nucl. Instr. and Meth. A 258 (1987) 431.
[12] J.F. Ritt, Differential Algebra, American Mathematical Society, Washington, DC, 1950.
[13] E.R. Kolchin, Differential Algebra and Algebraic Groups, Academic Press, New York, 1973.
[14] J.F. Ritt, Differential Equations from the Algebraic Viewpoint, American Mathematical Society, Washington, DC, 1932.
[15] K. Makino, Rigorous analysis of nonlinear motion in particle accelerators, Ph.D. Thesis, Michigan State University, East Lansing, Michigan, USA, 1998, Also MSUCL-1093.
[16] K. Makino, M. Berz, Int. J. Appl. Math. 3 (4) (2000) 421.
[17] K. Makino, M. Berz, Solenoid elements in COSY INFINITY, in: Proceedings Seventh International Computational Accelerator Physics Conference, IOP, East Lansing, MI, 2002.
[18] M.W. Garrett, J. Appl. Phys. 34 (9) (1963) 2567.
[19] R.C. Fernow, ICOOL: a simulation code for ionization cooling of muon beams, in: 1999 Particle Accelerator Conference, IEEE, New York, 1999, p. 3020.
[20] ICOOL at FNAL. http://www-pat.fnal.gov/muSim/icool.html/.
[21] A. Geraci, T. Barlow, M. Portillo, J. Nolen, K. Sheppard, M. Berz, K. Makino, Rev. Sci. Instr. 73 (9) (2002) 3174.
[22] A.A. Geraci, J.A. Nolen, R.C. Pardo. Superconducting linac beam dynamics with high-order maps for RF resonators, Nucl. Instr. and Meth., 2004, these proceedings.
[23] K.L. Brown, J.E. Spencer, IEEE Trans. on Nucl. Sci. NS-28 (3) (1981) 2568.
[24] D. Errede, K. Makino, M Berz, C.J. Johnstone, A. van Ginneken, Stochastic processes in muon ionization cooling, Nucl. Instr. and Meth., 2004, these proceedings.